INTERNATIONAL JOURNAL FOR NUMERICAL METHODS IN ENGINEERING, VOL. 24, 1461–1477 (1987)

FINITE ELEMENT ANALYSIS OF QUASI-PRISMATIC BODIES USING CHEBYSHEV POLYNOMIALS

SANDEEP M. VIJAYAKAR, HENRY R. BUSBY AND DONALD R. HOUSER

Gear Dynamics and Noise Research Laboratory, Department of Mechanical Engineering, The Ohio State University, Columbus, Ohio 43210, U.S.A.

SUMMARY

A new kind of finite element is presented in this paper which is designed to work efficiently for bodies that are either prismatic or 'quasi-prismatic' in shape. Quasi-prismatic shapes are those which can be obtained from prismatic shapes by mere distortion. The element which is formulated in this paper may be coupled with other types of three-dimensional elements to allow the modelling of structures which are only partially prismatic or which have prismatic shapes within them. The element allows for a variety of boundary conditions, yet yields meshes which are easy to generate. The performance of this element is evaluated by numerical experiments that compare its results with analytical solutions for a thick cylinder problem and a curved beam problem. The element has also been demonstrated on a turbine blade model.

INTRODUCTION

Finite element methods have been used for one-, two- and three-dimensional problems. Many engineering problems that are currently modelled with three-dimensional elements have cross-sections which remain constant or almost constant in one direction. These types of geometries, which include gear teeth, turbine blades, tires, wheels, pipes, springs, hooks and shafts, currently require numerous elements along the constant geometry direction in order to provide good aspect ratios and to adequately capture stress gradients at critical sections. This paper presents a method which can reduce the number of degrees of freedom required for such structures while capturing stress gradients with equal or better resolution. This method has the potential for exceptional computational efficiency. In addition, automatic mesh generation is greatly simplified. Because the geometry of the structures being modelled is almost prismatic, it is proposed to employ shape functions that are similar to a Fourier series of variable order in the direction of constant geometry.

Similar two-dimensional methods which use Fourier series expansions in one direction have been reported earlier.[1–6] Such approaches have been referred to in the literature as the finite strip methods and have been applied mainly to plate problems.

A three-dimensional method using Fourier series expansions in one direction along which material properties and geometry do not vary has also been reported.[7–9] The main application of this method, which has been referred to as the finite prism method, has been the analysis of bridge support prisms and box structures. The finite prism method has been used primarily in analysing prismatic structures constrained at either end. The main advantage cited for the method is that the prismatic geometry and the orthogonality of the Fourier terms and their derivatives cause the system stiffness matrix to become diagonal, thus reducing the effort required for

0029–5981/87/081461–17$08.50

Received 14 May 1986
Revised 17 October 1986

solution. This also means that the number of harmonics used is not limited by the memory.

An advantage that is not explicitly stated[7–9] is that by letting the number of Fourier terms at each node be different, a very easy method of controlling the number of degrees of freedom per unit length along the constant geometry direction can be obtained. This would make it much easier to generate a mesh containing varying size elements. Smaller elements could then have nodes which use more Fourier terms than nodes of larger elements, and the mesh could still be easily generated by a simple program.

In the formulation proposed here, a compromise has been struck between the inefficient meshes that the conventional finite element method is forced to use and the restrictions that the finite prism method imposes. The stiffness matrix is not diagonal as in the finite prism method.

For reasons of computational efficiency, it was decided to choose a series of functions other than the Fourier series to approximate displacements. The method is generalized to allow either free or fixed ends, and to allow several elements to be compatible so that they could be assembled end to end. These new elements are also capable of being assembled with ordinary three dimensional finite elements (such as the isoparametric serendipity element[8]).

In order to be able to model a geometry such as the teeth of helical and spiral bevel gears, the nodal coordinates are also expanded as a series of variable order. The shape functions used are based on an orthogonal set of functions so that it is easier to expand coordinates and forces in terms of these shape functions.

For several reasons which are discussed below, a series of Chebyshev polynomials has been chosen. It has been shown[10] that the Chebyshev expansion is better behaved than any other member of the family of ultraspherical expansions. This family includes most polynomials frequently encountered which are orthogonal over the interval $[-1, +1]$. The Legendre expansion, Taylor series and an expansion in terms of Chebyshev polynomials of the second kind are also members of this family. In this class of polynomials, Chebyshev polynomial expansions yield a truncation error curve nearest to the desired equal-ripple form and yield expansions which display the strongest possible convergence.[11] One of the most important features[12] of the Chebyshev series is that, unlike the Fourier series, its convergence is not affected by the values of the function being approximated at the boundaries of the interval $[-1, +1]$. In contrast, the Gibbs phenomenon shows that the rate of convergence of the Fourier series depends on the value of the function and its derivatives at the boundaries. A term of a Chebyshev expansion can be exactly computed with a finite number of multiplications, unlike terms of the sine and cosine series. The Chebyshev polynomials are orthogonal and any integrable function can be decomposed into a Chebyshev expansion. Chebyshev quadrature can be used to compute coefficients. Finally, Chebyshev polynomials have been used with much success in fluid mechanics problems.[13,14]

Because of the nature of the element described in this paper, it will henceforth be referred to as the 'FQP' (Finite Quasi-Prism) element. Table I summarizes the salient features of this method in contrast to the conventional 3D finite element method and the finite prism method.

FORMULATION OF THE FINITE QUASI-PRISM (FQP) ELEMENT

(*a*) *Interpolation scheme*

The formulation of the FQP element is very similar to conventional finite elements, the difference being in the shape functions used.

The coordinates are approximated by

Table I. Salient features of the FQP element compared to the finite prism and the conventional 3D element

Finite prism	3D finite element	FQP element
Limited to prismatic geometries	No limitation	Limited to quasi-prismatic geometries
Stiffness matrix is diagonal	Not diagonal	Not diagonal
Number of harmonics not limited by memory	—	Number of terms in expansion limited by memory
Mesh creation is very easy	Mesh creation is very difficult	Mesh creation is much easier than 3D FE
Ends of finite prism have to be fixed	No such limitation	No such limitation
Cannot be combined in the same mesh with conventional finite elements	—	Can be combined in the same mesh with conventional finite elements

$$
\begin{aligned}
x(\xi,\eta,\zeta) &= \sum_{i=1}^{\mathrm{nc}} \sum_{j=0}^{\mathrm{no}(i)} x_{ij} N_i(\xi,\eta) T_j(\zeta) \\
y(\xi,\eta,\zeta) &= \sum_{i=1}^{\mathrm{nc}} \sum_{j=0}^{\mathrm{no}(i)} y_{ij} N_i(\xi,\eta) T_j(\zeta) \\
z(\xi,\eta,\zeta) &= \sum_{i=1}^{\mathrm{nc}} \sum_{j=0}^{\mathrm{no}(i)} z_{ij} N_i(\xi,\eta) T_j(\zeta)
\end{aligned} \tag{1}
$$

where nc is the number of 'axode' curves per element (see Figure 1), and no (i) is the order of the Chebyshev expansion at axode i. The displacements are interpolated in a very similar fashion:

$$
\begin{aligned}
u(\xi,\eta,\zeta) &= \sum_{i=1}^{\mathrm{nc}} \sum_{j=0}^{\mathrm{no}(i)} u_{ij} N_i(\xi,\eta) T_j(\zeta) \\
v(\xi,\eta,\zeta) &= \sum_{i=1}^{\mathrm{nc}} \sum_{j=0}^{\mathrm{no}(i)} v_{ij} N_i(\xi,\eta) T_j(\zeta) \\
w(\xi,\eta,\zeta) &= \sum_{i=1}^{\mathrm{nc}} \sum_{j=0}^{\mathrm{no}(i)} w_{ij} N_i(\xi,\eta) T_j(\zeta)
\end{aligned} \tag{2}
$$

The orders of interpolation for displacements do not have to be the same as for co-ordinates, but have been kept the same for reasons of programming convenience. The $N_i(\xi,\eta)$ are

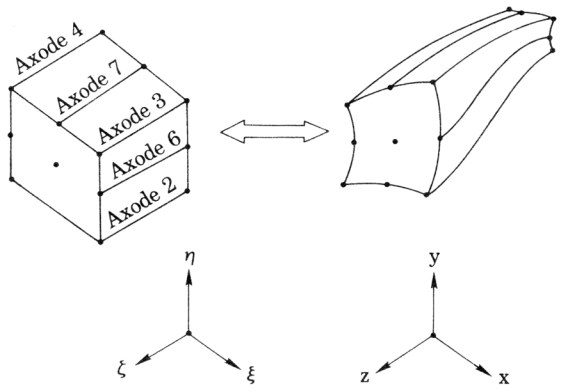

Figure 1. Mapping from local coordinates to global coordinates

two-dimensional Lagrangian shape functions for isoparametric elements with the number of nodes capable of varying between three and nine.

The $T_j(\zeta)$ are shape functions derived from Chebyshev polynomials:

$$T_0(\zeta) = (1-\zeta)/2, \quad T_1(\zeta) = (1+\zeta)/2, \quad T_2(\zeta) = \tau_2(\zeta) - 1$$
$$T_3(\zeta) = \tau_3(\zeta) - \zeta, \quad T_4(\zeta) = \tau_4(\zeta) - 1$$
$$\vdots$$
$$T_n(\zeta) = \begin{cases} \tau_n(\zeta) - 1 & \text{for} \quad n > 1 \quad \text{and} \quad \text{even} \\ \tau_n(\zeta) - \zeta & \text{for} \quad n > 1 \quad \text{and} \quad \text{odd} \end{cases}$$

The $\tau_n(\zeta)$ are Chebyshev polynomials defined by

$$\tau_0(\zeta) = 1, \quad \tau_1(\zeta) = \zeta, \quad \tau_2(\zeta) = 2\zeta^2 - 1$$
$$\tau_3(\zeta) = 4\zeta^3 - 3\zeta, \quad \tau_4(\zeta) = 8\zeta^4 - 8\zeta^2 + 1$$
$$\tau_5(\zeta) = 16\zeta^5 - 20\zeta^3 + 5\zeta$$

or,

$$\tau_n(\zeta) = t_0^{(n)} + t_1^{(n)}\zeta + \cdots + t_n^{(n)}\zeta^n$$

where

$$t_{n-(2k+1)}^{(n)} = 0; \quad k = 0, \ldots, \left[\frac{n-1}{2}\right]$$

and

$$t_{n-2k}^{(n)} = (-1)^k \sum_{j=k}^{[n/2]} \binom{n}{2j}\binom{j}{k}; \quad k = 0, \ldots, [n/2]$$

where

$$\binom{n}{r} = \frac{n!}{r!(n-r)!} \quad \text{and} \quad [n/2] = \text{the integral value of } n/2$$

(*b*) *Properties of Chebyshev polynomials*

Some properties of the Chebyshev polynomials are

$$\tau_n(+1) = +1$$

$\tau_n(-1) = +1$ or -1 depending on whether n is even or odd respectively.

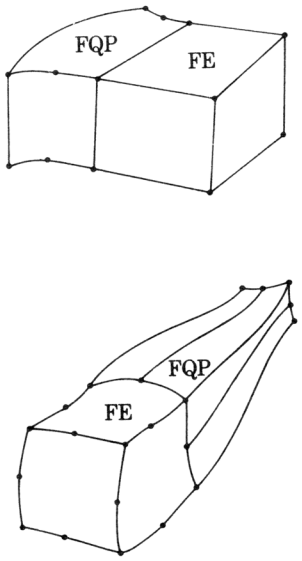

Figure 2. Assembly of finite 'quasi'-prism elements with conventional finite elements

Hence,

$$T_0(-1)=1, \quad T_n(-1)=0 \quad \text{for all} \quad n>0$$

$$T_1(+1)=1, \quad T_n(+1)=0 \quad \text{for} \quad n=0 \quad \text{or} \quad n>1$$

so that $\zeta=-1$ is a 'node' for the shape function T_0, $\zeta=+1$ is a 'node' for the shape function T_1 and the shape functions $T_2, T_3, T_4, \ldots$ are nodeless and disappear at $\zeta=\pm 1$. This property makes it possible to assemble these elements end to end and if only a linear expansion is chosen, these elements can be assembled alongside a linear finite element (see Figure 2).

$\tau_n(\zeta)$ has n zeros, all between -1 and 1. The jth zero of $\tau_n(\zeta)$ is

$$\zeta_j^{(n)}=\cos\left(\frac{(2j-1)\pi}{2n}\right) \quad \text{for} \quad j=1,2\ldots,n$$

The Chebyshev polynomials are a complete and orthogonal set with respect to the weight function $1/(1-\zeta^2)^{1/2}$ within the interval $[-1,1]$ such that

$$\int_{-1}^{+1}\frac{\tau_n(\zeta)\tau_m(\zeta)}{(1-\zeta^2)^{1/2}}\,\mathrm{d}\zeta=\begin{cases}\pi \text{ if } n=m=0\\ \dfrac{\pi}{2} \text{ if } n=m>0\\ 0 \text{ otherwise}\end{cases}$$

The roots of the Chebyshev polynomials can be used for quadrature

$$\int_{-1}^{+1}\frac{f(\zeta)}{(1-\zeta^2)^{1/2}}\,\mathrm{d}\zeta=\frac{\pi}{n}\sum_{j=1}^{n}f(\zeta_j^{(n)}) \quad \text{for all.} \quad f\in P_{2n-1}$$

Figure 3 shows plots of the shape functions $T_0(\zeta)$ to $T_5(\zeta)$.

Along any one of the axode curves $(\xi,\eta)=(\xi_k,\eta_k)$ that describe an element,

$$x(\xi_k,\eta_k,\zeta)=\sum_{i=1}^{\mathrm{nc}}\sum_{j=0}^{\mathrm{no}(i)}x_{ij}N_i(\xi_k,\eta_k)T_j(\zeta)$$

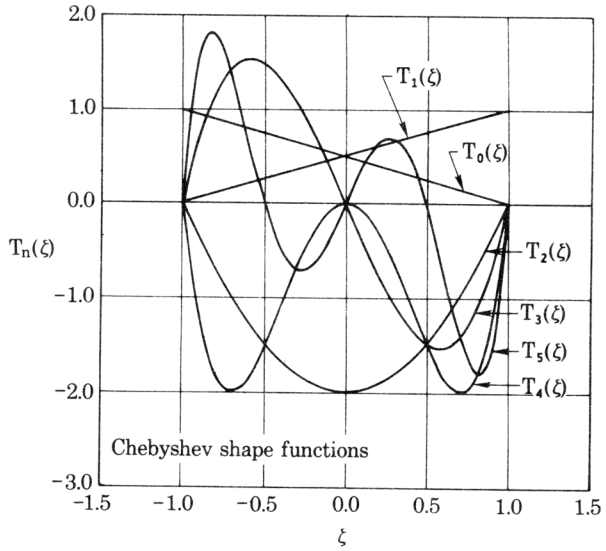

Figure 3. The shape functions based on Chebyshev polynomials

$$= \sum_{j=0}^{\mathrm{no}(k)} x_{kj} T_j(\zeta)$$

Similarly,

$$y(\xi_k, \eta_k, \zeta) = \sum_{j=0}^{\mathrm{no}(k)} y_{kj} T_j(\zeta) \quad \text{and} \quad z(\xi_k, \eta_k, \zeta) = \sum_{j=0}^{\mathrm{no}(k)} z_{kj} T_j(\zeta)$$

The x_{kj}, y_{kj} and z_{kj} are nodal coordinates (or nodeless coordinates for $k > 1$) which have to be determined while generating the FQP model. The property of orthogonality of Chebyshev polynomials is of use at this stage. Let $f(\zeta)$, $-1 \leqslant \zeta \leqslant +1$ be a function that is to be expanded in terms of the shape functions $T_j(\zeta)$ where $j = 0, 1, 2, \ldots, n$. Then,

$$f(\zeta) = \sum_{j=0}^{\infty} a_j \tau_j(\zeta) \quad \text{where} \quad a_j = \frac{\langle f, \tau_j \rangle}{\| \tau_j \|^2}$$

$$\langle f, g \rangle = \int_{-1}^{+1} \frac{f(\zeta) g(\zeta)}{(1-\zeta^2)^{1/2}} \, \mathrm{d}\zeta$$

and

$$\| \tau_j \|^2 = \begin{cases} \pi & \text{if } j = 0 \\ \dfrac{\pi}{2} & \text{otherwise} \end{cases}$$

The integral can be approximated by

$$\langle f, \tau_j \rangle = \int_{-1}^{+1} \frac{f(\zeta) \tau_j(\zeta)}{(1-\zeta^2)^{1/2}} \, \mathrm{d}\zeta = \frac{\pi}{n} \sum_{k=1}^{n} f(\zeta_k^{(n)}) \tau_j(\zeta_k^{(n)})$$

which is exact if $f \in P_{2n-1-j}$. Thus

$$f(\zeta) = \sum_{j=0}^{\infty} a_j \tau_j(\zeta) = \sum_{j=0}^{\infty} f_j T_j(\zeta) \tag{3}$$

Since $\tau_j(\zeta)$ and $T_j(\zeta)$ differ only by ζ or by 1 for $j > 1$,

$$f_j = a_j = \frac{\langle f, \tau_j \rangle}{\| \tau_j \|^2}, \quad \text{for} \quad j > 1$$

Substituting $\zeta = -1$ and $+1$ respectively in (3),

$$f_0 = f(-1) \quad \text{and} \quad f_1 = f(+1)$$

(c) *Finite element formulation*

Equation (2) can also be written in vector form as

$$\mathbf{u}(\xi, \eta, \zeta) = \sum_{i=1}^{\text{nc}} \sum_{j=0}^{\text{no}(i)} \mathbf{u}_{ij} N_i(\xi, \eta) T_j(\zeta)$$

where

$$\mathbf{u} = (u, v, w)^{\mathrm{T}} \quad \text{and} \quad \mathbf{u}_{ij} = (u_{ij}, v_{ij}, w_{ij})^{\mathrm{T}}$$

In matrix notation these become

$$\mathbf{u} = [N]\{a\} \tag{4}$$

where

$$\{a\} = (\mathbf{u}_{11}, \mathbf{u}_{12}, \ldots, \mathbf{u}_{1\,\text{no}(1)}, \mathbf{u}_{21}, \ldots, \mathbf{u}_{\text{nc,no(nc)}})^{\mathrm{T}}$$

The expression for strains is obtained by differentiating the displacements

$$\{\varepsilon\} = [L]\mathbf{u} = [L][N]\{a\} = [B]\{a\}$$

where $[L]$ is the matrix differential operator[8] relating strains to displacements. The general finite element equations may then be obtained in the usual manner, in this case using the Galerkin form of the weighted residual method to get

$$\int_V [B]^{\mathrm{T}}[D][B]\,\mathrm{d}V\{a\} = \int_V [N]^{\mathrm{T}}\mathbf{b}\,\mathrm{d}V$$

or

$$[K]\{a\} = \{f\}$$

where $[D]$ is the elasticity matrix, $\mathbf{b}$ is the applied load intensity vector, $[K]$ is the system stiffness matrix and $\{f\}$ is the system load vector.

Integration is carried out numerically by Gaussian quadrature using a $3 \times 3 \times ngpz$ rule, where $ngpz$ is the number of Gauss points in the ζ direction:

$$ngpz = 1 + \max_{i=1,\text{nc}} (\text{no}\,(i)) \text{ for each element}$$

NUMERICAL EXAMPLES

A program implementing the FQP element was written to run on a VAX-11/750 in FORTRAN. An in-core skyline solution program was used to solve the system of equations. It is intended to implement an out-of-core solution routine in the future to enable the solution of larger problems.

In order to demonstrate the FQP element, three example cases were chosen. The classic thick cylinder problem was used because, by reducing the inner radius of the thick cylinder, severe stress gradients can be created. In addition, the thick cylinder problem is essentially a one-dimensional problem, in that no gradients exist in the circumferential and axial directions, thus making possible a complete graphic presentation of the results. The second example, a

curved beam problem, is used because an exact solution is available for comparison and because there are two ways in which it can be modelled by the FQP element, thus giving the opportunity for exploration of the performance of the element. Finally, as a third example, a turbing blade stress analysis problem is considered since it is typical of the class of problems that the FQP element is designed for.

(*a*) *Thick cylinder subjected to internal pressure*

Consider a thick cylinder having an internal radius, a, and an external radius, b (see Figure 4). The exact solution to the thick cylinder problem is given by Spotts.[15] The displacements vary as $1/r$ and the stresses vary as $1/r^2$ as the ratio a/b tends to zero. For this example, the a/b ratio was chosen to be 0·1 so that sufficiently high stress gradients are created near the inner radius. Poisson's ratio, ν, was chosen to be 0·3.

Figure 5 shows an FQP mesh that uses two elements. The ζ direction for both elements is along the radius of the cylinder. Quadratic interpolation is used for both elements along the circumferential direction and linear interpolation is used in the axial direction. Figure 6 shows the displacements obtained with Chebyshev interpolation of orders one, three and six respectively, along the ζ (radial) direction and Figures 7 and 8 show the corresponding stresses which were calculated. The order 6 interpolation fits the exact displacements very well (with a maximum

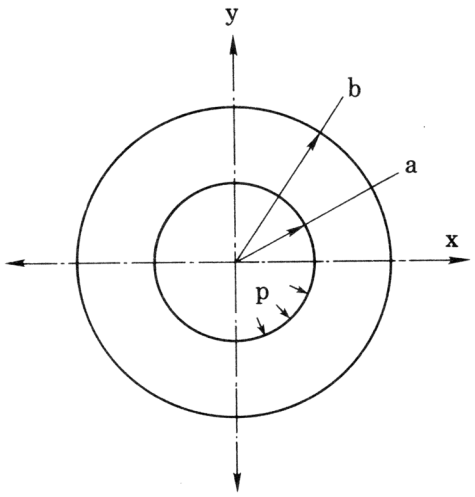

Figure 4. Thick cylinder subjected to internal pressure

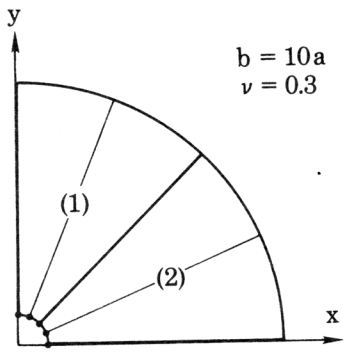

Figure 5. FQP mesh used for the thick cylinder

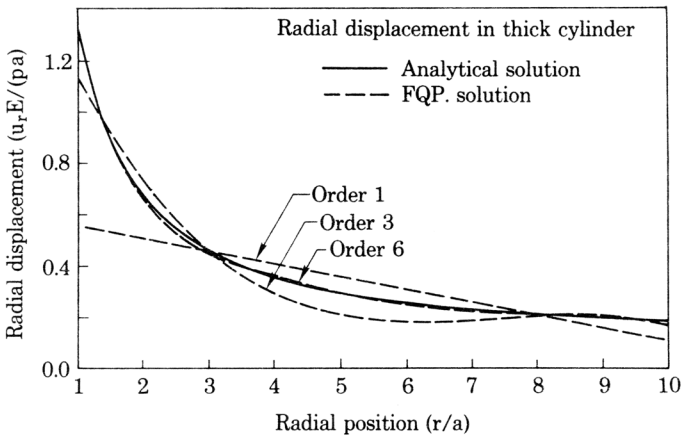

Figure 6. Comparison of displacements from the FQP mesh with the exact displacements

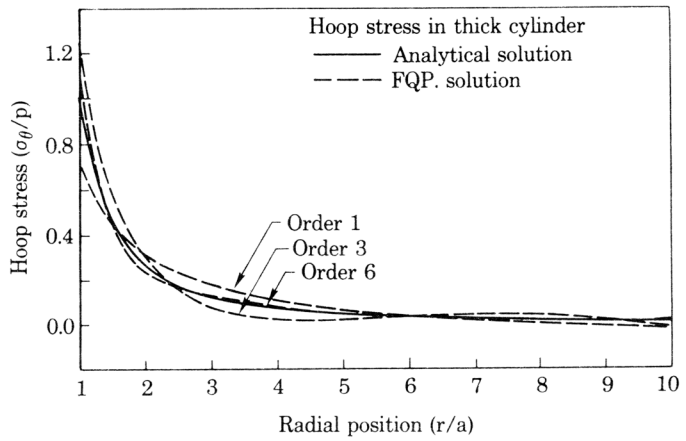

Figure 7. Comparison of hoop stresses from the FQP mesh with the exact stresses

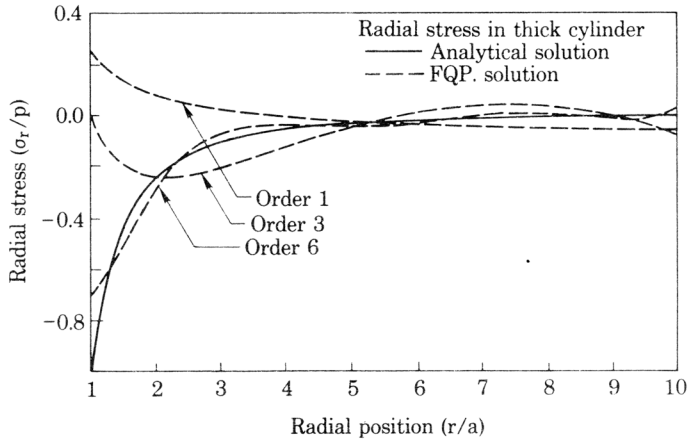

Figure 8. Comparison of radial stresses from the FQP mesh with the exact stresses

error of 1·5 per cent of the maximum displacement). The order 1 interpolation fits the exact curve about as well as can be expected for a straight line fit.

The calculated stress curves were found to intersect the exact stress curves very near the Gauss points of the same order as the curve. For example, the order 1 hoop stress and radial stress curves intersect the exact stress curves very near the order 1 Gauss point ($\zeta = 0{\cdot}0$). The order 6 stress curves intersect the corresponding exact stress curves very near the six Gauss points of order 6. The maximum error of the hoop stresses calculated at the Gauss points for the order 6 approximation was 1·324 per cent of the maximum hoop stress and for the radial stresses, the maximum Gauss point error was 1·331 per cent of the maximum radial stress.

(*b*) *Curved beam*

For a thick curved beam in a state of plane stress loaded by shear on one end, as shown in Figure 9, an exact solution is given by Timoshenko and Goodier.[16]

Figures 10 and 11 show two FQP meshes used to model the curved beam. Figure 10 shows a mesh consisting of two FQP elements, with their ζ directions along the radial direction of the beam. A fourth order Chebyshev shape function interpolation was used in this direction. Each element used quadratic interpolation along the circumferential direction and linear interpolation along the z direction. The thickness of each element in the z direction was kept very small in order to model plane stress properly. Figure 11 shows a second mesh consisting of two FQP elements having their ζ directions along the circumferential direction of the curved beam. A fourth order Chebyshev shape function interpolation is used in that direction. Figures 12, 13 and 14 show contours of displacement in the Y directions for meshes (a), (b) and for the exact solution, respectively. Figures 15, 16 and 17 give contours of displacement in the X directions for the same cases. Both meshes give smaller displacements than the exact solution. The displacement contours of mesh (b) match almost exactly those of the exact solution and mesh (a) is much stiffer that mesh (b). Figures 18, 19 and 20 show the respective contours of the von Mises octahedral shear stresses from meshes (a), (b) and the exact solution. Because the shape functions provide only C_0 continuity of displacements, the stresses computed are not continuous

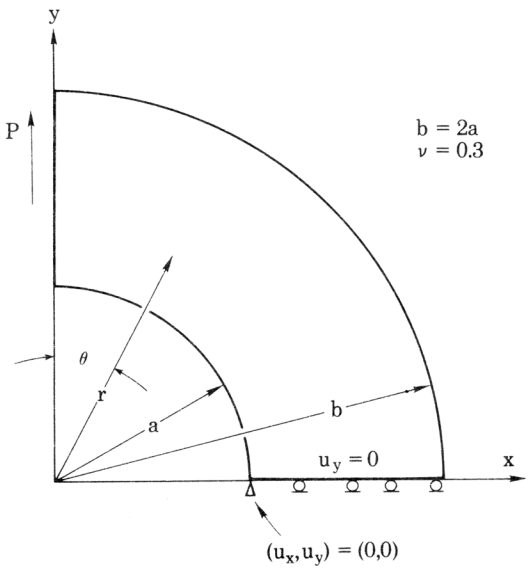

Figure 9. Curved beam loaded on one end by a shear stress

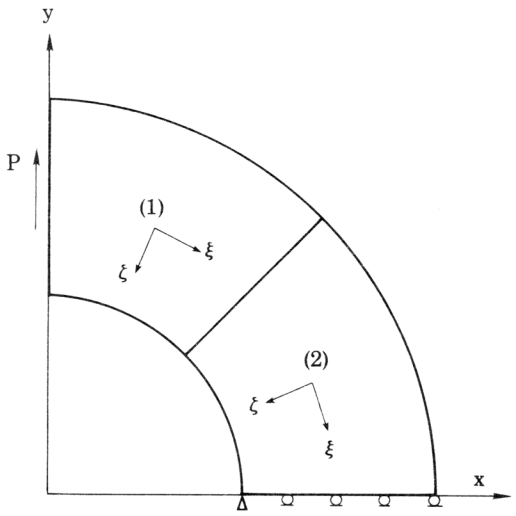

Figure 10. Curved beam mesh (a)

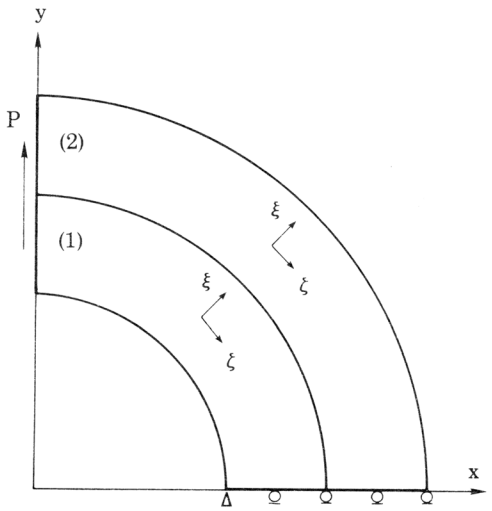

Figure 11. Curved beam mesh (b)

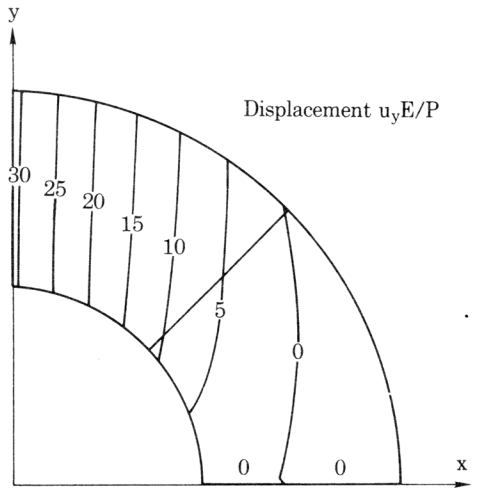

Figure 12. Displacement u_y contours in mesh (a)

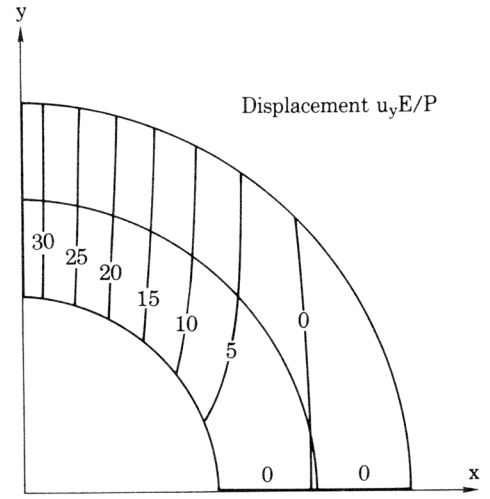

Figure 13. Displacement u_y contours in mesh (b)

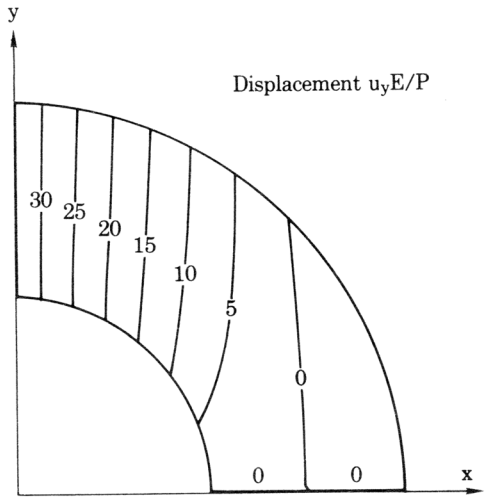

Figure 14. Displacement u_y contours from the exact solution

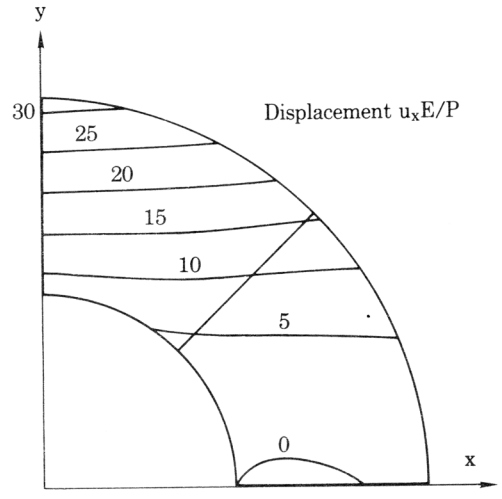

Figure 15. Displacement u_x contours in mesh (a)

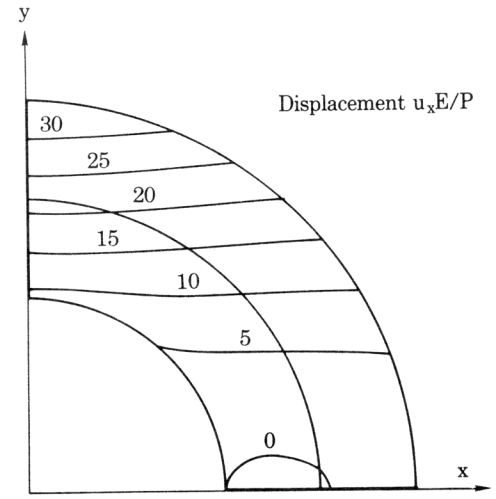

Figure 16. Displacement u_x contours in mesh (b)

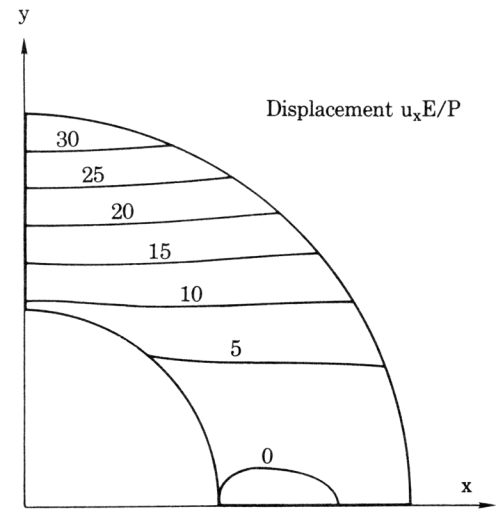

Figure 17. Displacement u_x contours from the exact solution

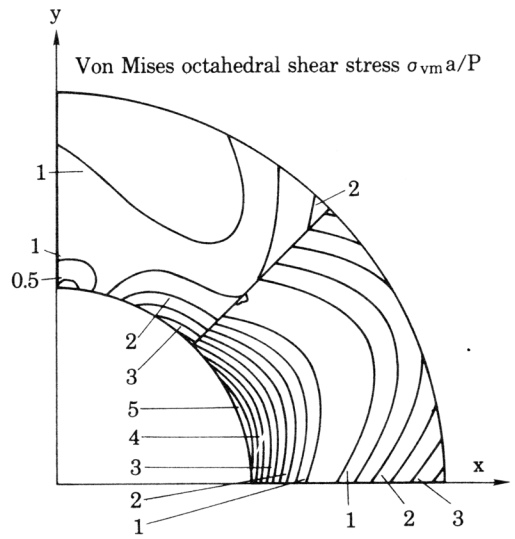

Figure 18. Von Mises octahedral shear stress contours in mesh (a)

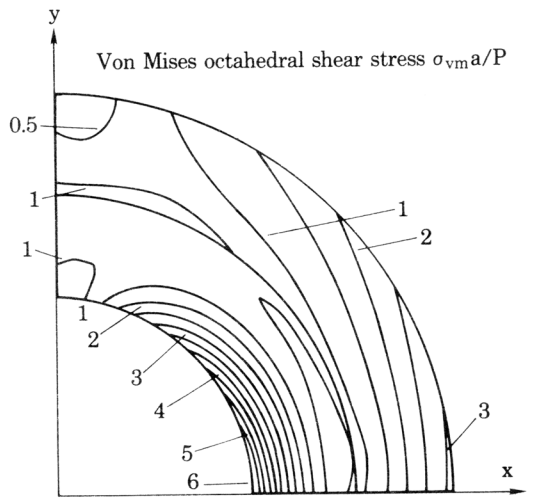

Figure 19. Von Mises octahedral shear stress contours in mesh (b)

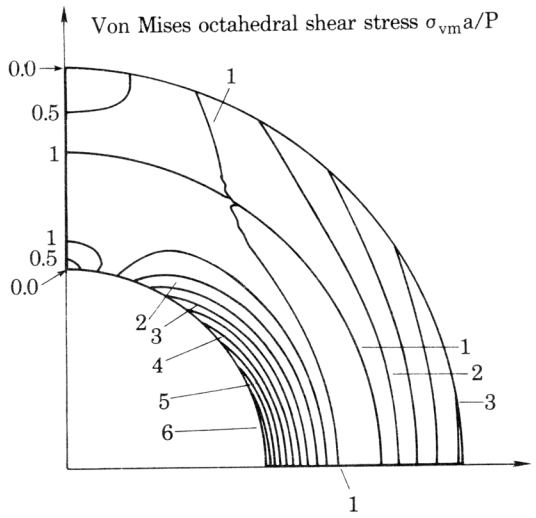

Figure 20. Von Mises octahedral shear stress contours from the exact solution

across element boundaries. Looking at these stress contours gives a clue as to why mesh (b) gives more accurate results. The reason, as evidenced in the stress contour plots, is that mesh (b) can conform more easily to the stress gradients in this particular problem than mesh (a). This is despite the fact that both meshes have the same number (five) of 'nodes' (real or virtual) in both the radial and circumferential directions. This shows clearly that there is a need for more research into the behaviour of the FQP element.

(*c*) *Turbine blade model*

Figure 21 shows a full three-dimensional model of a turbine blade and its root. The blade is loaded by a uniform pressure P on its concave side. The boundaries of the 'christmas tree' root are constrained from moving in any direction. The model has a total of 2340 degrees of freedom and a bandwidth of 621. The ζ direction of the FQP elements is along the Y direction. The

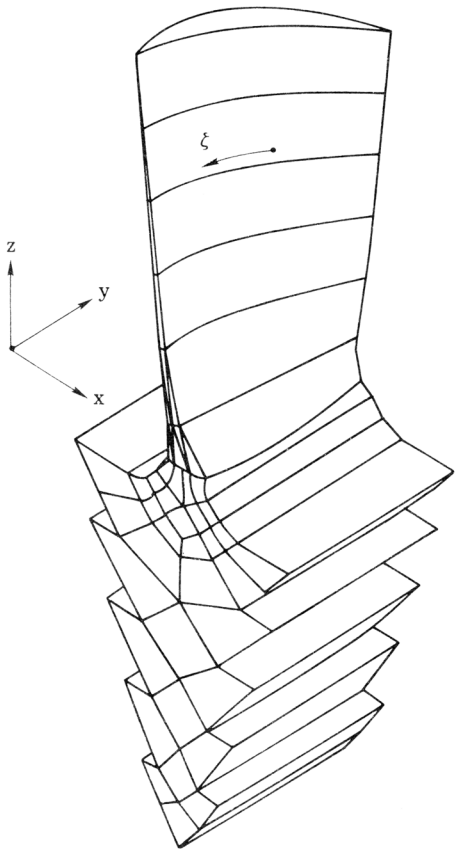

Figure 21. A turbine blade model using FQP elements

'neck' region where the blade joins the root is where the stresses are of most interest. Most of the degrees of freedom (1569 out of 2340) are concentrated in this region. Chebyshev shape functions of order 10 are used in this region, as compared to orders 3 and 6 elsewhere. Had conventional finite elements been used, the transition from 11 nodes in the Y direction at the neck to 4 nodes along the Y direction at the tip of the blade and at the bottom of the root would have immensely complicated mesh generation and would have used more degrees of freedom. Figures 22(a) to 22(c) show contours of constant octahedral shear stress at three selected sections of the elements at the neck of this model. It should be noted that the stresses are discontinuous at the interelement boundaries and that these discontinuities have been preserved in the contour plots to show the actual behaviour of the FQP elements.

CONCLUSIONS

This paper has shown that the FQP element can be a very efficient and accurate alternative to conventional finite elements and offers a definite advantage over finite elements for a whole class of problems. The authors are convinced of the practicality of these elements and of their potential for computational savings. A detailed comparison between the FQP elements and conventional 3D finite elements needs to be carried out to show that using a 'theoretically best' basis of shape functions gives more accurate results than conventionally used shape functions. Since these elements can be made to interface with normal finite elements, they can be used to advantage,

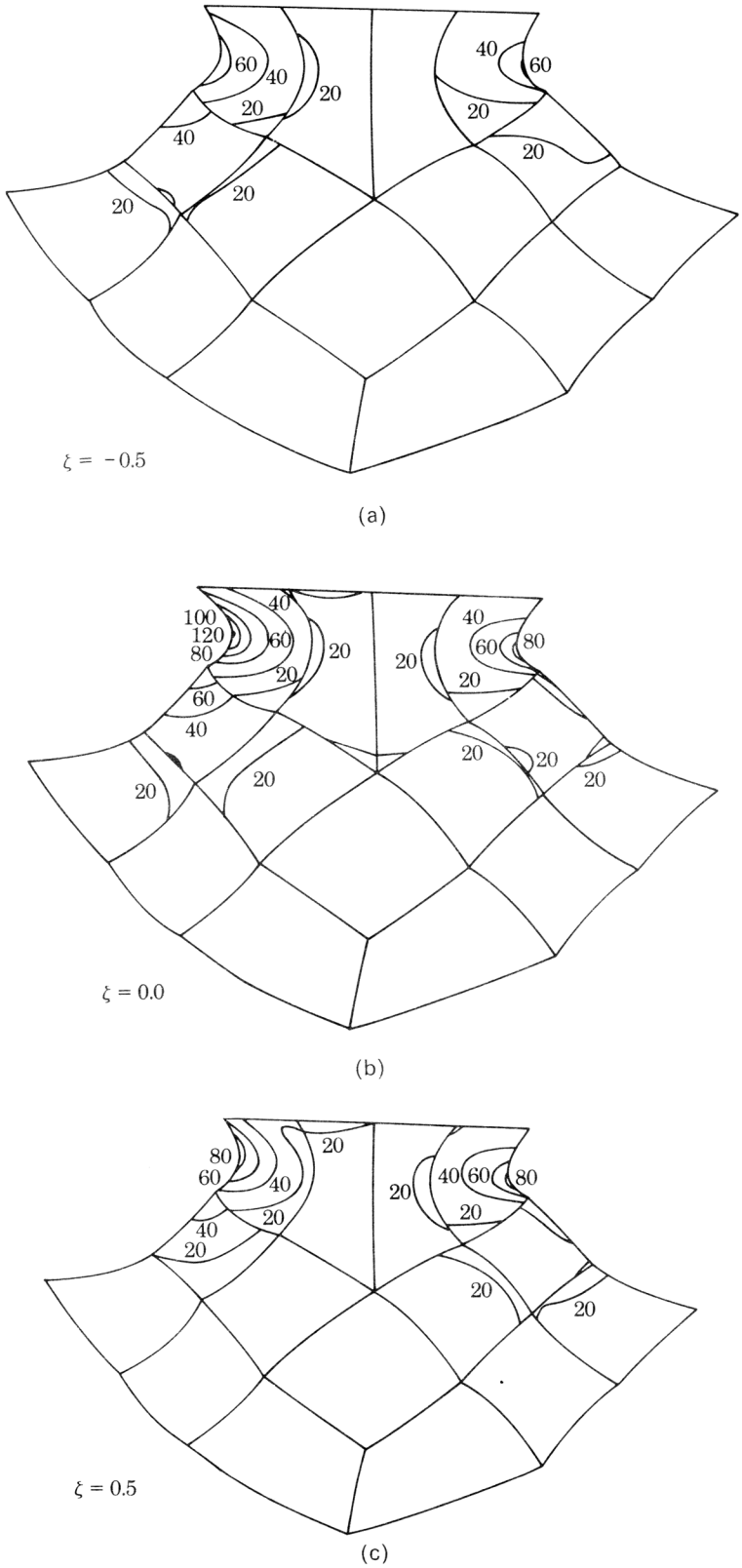

Figure 22. Contours of von Mises octahedral stress σ_{vm}/P at selected sections within the turbine blade model

even if only used in portions of the model. Much of the development, remarks and conclusions would apply also to heat conduction and similar field problems.

Finally, there is a need for theoretical error and convergence rate estimates. Such estimates should help in deciding *a-priori* how many terms are needed in FQP models.

ACKNOWLEDGEMENTS

The authors are grateful to the sponsors of the Gear Dynamics and Noise Research Laboratory of The Ohio State University for their financial support and to the Advanced Design Methods Laboratory of The Ohio State University for the use of its computer facilities.

REFERENCES

1. P. Lengyel and A. R. Cusens, 'A finite strip method for the analysis of plate structures', *Int. j. numer. methods eng.*, **19,** 331–340 (1983).
2. Kenneth Runesson and John R. Booker, 'Finite element analysis of elastic–plastic layered soil using discrete Fourier series expansion', *Int. j. numer. methods eng.*, **19,** 473–478 (1983).
3. Srinivasan Sridharan, 'A semianalytical method for the post-local-torsional buckling analysis of prismatic plate structures', *Int. j. numer. methods eng.*, **18,** 1685–1697 (1982).
4. D. J. Dawe, 'Static analysis of diaphragm supported cylindrical shells using a curved finite strip', *Int. j. numer. methods eng.*, **11,** 1347–1364 (1977).
5. R. R. Benson and E. Hinton, 'A thick finite strip solution for static free vibration and stability problems', *Int. j. numer. methods eng.*, **10,** 665–678 (1976).
6. R. J. Plank and W. H. Wittrick, 'Buckling under combined loading of thin, flat walled structures by a complex finite strip method', *Int. j. numer. methods eng.*, **8,** 323–339 (1974).
7. Carlos C. K. Wong and Alan E. Wardy, 'Finite prism analysis of plates and shells', *Int. j. numer. methods eng.*, **21,** 529–541 (1985).
8. O. C. Zienkiewicz, *The Finite Element Method, 3rd edn.*, McGraw-Hill, 1979.
9. O. C. Zienkiewicz and J. J. M. Too, 'The finite prism in analysis of thick simply supported bridge boxes', *Proc. Inst. Civil Eng.*, **53,** 147–172 (1972).
10. Theodore J. Rivlin, *The Chebyshev Polynomials*, Wiley–Interscience, New York, 1974.
11. Martin Avery Snyder, *Chebyshev Methods in Numerical Approximation*, Prentice-Hall, Englewood Cliffs, N.J., 1966.
12. M. F. Gottlieb and S. A. Orszag, *Numerical Analysis of Spectral Methods. Regional Conference Series in Applied Mathematics*, Society for Industrial and Applied Mathematics, 1977.
13. D. B. Haidvogel and T. Zang, 'The accurate solution of Poisson's equation by expansion in Chebyshev polynomials', *J. Comp. Phys.*, **30,** 167–180 (1979).
14. P. S. Marcus, 'Simulation of Taylor–Couette flow. Part I. Numerical methods and comparison', *J. Fluid Mech.*, **146,** 45–64 (1984).
15. M. F. Spotts, *Design of Machine Elements, 5th edn.*, Prentice-Hall, Englewood Cliffs, N.J., 1978.
16. S. P. Timoshenko and J. N. Goodier, *Theory of Elasticity*, McGraw-Hill, London, 1970.